Delft University of Technology

Effect of time stepping strategy on adjoint-based production optimization

Volkov, O.; Voskov, D. V.

DOI
10.1007/s10596-015-9528-1

Publication date
2016

Document Version
Final published version

Published in
Computational Geosciences: modeling, simulation and data analysis

Citation (APA)
Volkov, O., & Voskov, D. V. (2016). Effect of time stepping strategy on adjoint-based production optimization. *Computational Geosciences: modeling, simulation and data analysis*, *20*(3), 707-722. https://doi.org/10.1007/s10596-015-9528-1

Important note
To cite this publication, please use the final published version (if applicable).
Please check the document version above.

Copyright
Other than for strictly personal use, it is not permitted to download, forward or distribute the text or part of it, without the consent of the author(s) and/or copyright holder(s), unless the work is under an open content license such as Creative Commons.

Takedown policy
Please contact us and provide details if you believe this document breaches copyrights.
We will remove access to the work immediately and investigate your claim.

This work is downloaded from Delft University of Technology.
For technical reasons the number of authors shown on this cover page is limited to a maximum of 10.

Comput Geosci (2016) 20:707–722
DOI 10.1007/s10596-015-9528-1

ORIGINAL PAPER

Effect of time stepping strategy on adjoint-based production optimization

O. Volkov[1] · D. V. Voskov[2]

Received: 30 October 2014 / Accepted: 7 September 2015 / Published online: 25 September 2015
© Springer International Publishing Switzerland 2015

Abstract The adjoint gradient method is well recognized for its efficiency in large-scale production optimization. When implemented in a sequential quadratic programming (SQP) algorithm, adjoint gradients enable the construction of a quadratic approximation of the objective function and linear approximation of the nonlinear constraints using just one forward and one backward simulation (with multiple right-hand sides). In this work, the focus is on the performance of the adjoint gradient method with respect to the adaptive time step refinement generated in the underlying forward simulations. First, we demonstrate that the mass transfer in reservoir simulation and, as a consequence, the net-present value (NPV) function are more sensitive to the degree of the time step refinement when using production bottom-hole pressure (BHP) controls than when using production rate controls. Effects of this sensitivity on optimization process are studied using six examples of uniform time stepping with different degrees of refinements. By comparing those examples, we show that corresponding optimal solutions for target production BHPs deviate at early stages of the optimization process. It indicates an inconsistency in the evaluation of the adjoint gradients and NPV function for different time step refinements. Next, we investigate the effects of this inconsistency on the results of a constrained production optimization. Two strategies of nonlinear constraints are considered: (i) nonlinear constraints handled in the optimization process and (ii) constraints applied directly in forward simulations with a common control switch procedure. In both strategies, we observe that the progress of the optimization process is greatly influenced by the degree of the time step refinement after control update. In the case of constrained simulations, the presence of control switches combined with large time steps after control update forces adaptive refinement to vary the time step size significantly. As a result, the inconsistency of the adjoint gradients and NPV values provoke an early termination of the SQP algorithm. In the case of constrained optimization, the inconsistencies in gradient evaluations are less significant, and the performance of the optimization process is governed by a satisfaction of nonlinear constraints in SQP algorithm.

Keywords Reservoir simulation · Adjoint gradient · Production optimization · Time step sensitivity

Mathematics Subject Classification (2010) 35Q93 · 76N25 · 86A22 · 90C06

✉ O. Volkov
ovolkov@stanford.edu

D. V. Voskov
d.v.voskov@tudelft.nl

[1] Department of Energy Resources Engineering, Stanford University, 367 Panama Street, Stanford, CA 94305, USA

[2] Civil Engineering & Geosciences, Delft University of Technology, Stevinweg 1, 2628 CN Delft, The Netherlands

1 Introduction

As the capabilities of reservoir simulators grow, it is becoming possible to solve a reservoir optimization problem of great complexity. Large realistic reservoir models require massive computational resources, which can be mitigated using efficient computational optimization algorithms. The reservoir production optimization can be cast as a constrained optimization problem where the majority of constraints has the form of partial differential equation (PDE).

In this class of optimization problems, efficiency is often achieved by using an adjoint-based gradient method implemented within the nonlinear programming (NLP) algorithm. Among NLP algorithms, sequential quadratic programming (SQP) and method of moving asymptotes (MMA) have been applied successfully to solve production optimization problems [2, 20]. This work concentrates only on the SQP algorithm since it has a long history in solving optimal well control problems and has proven to be highly efficient [1].

The SQP algorithm finds a local optimum of a constrained optimization problem by solving a sequence of quadratic programming (QP) problems where the objective function and constraints are approximated by quadratic and linear models, respectively. To improve the accuracy and efficiency of these models, the adjoint gradient method is applied. This method serves to eliminate PDE constraints and calculates the total variation of the objective function and remaining non-PDE constraints, with respect to the optimization variables. It is accomplished by calculating sensitivities of the objective function with respect to the PDE constraints, called adjoint variables [16, 18]. For a given state of the reservoir, the adjoint variables can be accurately computed using one backward in time simulation with a linearized reservoir system.

To build a quadratic model of the objective function, the SQP algorithm uses an approximation of the second-order sensitivity (Hessian) of the objective function with respect to the optimization variables. The approximation of the Hessian is assembled from objective gradients computed at several optimization iterations and, therefore, relies on the consistency of the gradients among simulations. The Hessian represents information about the curvature of an objective function. If its estimation is inaccurate, it might wrongly shape the optimum search space and not allow the solution to converge, i.e., to satisfy the Karush–Kuhn–Tucker conditions [13].

The theoretical studies of how the gradient consistency affects the performance of the SQP algorithm are often limited to the cases of smooth and convex objective functions. For example, in [4], the authors prove theoretically that the SQP algorithm fails to converge when the relative error of the gradient is above 50 %. Obviously, the analysis detailed in [4] cannot be readily replicated in the case of a general production optimization problem. Instead, in this work, we design a numerical experiment that induces the commonly observed gradient errors and study their impact on the optimization process.

The adjoint gradients may have large errors in realistic production optimization problems, due to the following reasons:

(i) Inaccurate partial derivatives in the linearization of the reservoir equation system

Multiphase fluid mass balance in the reservoir is modeled by highly nonlinear conservation equations representing volume-averaged flow. The model parameters are often determined through experimental studies and, therefore, lack smoothness. Nondifferentiability of model parameters and phase appearance/disappearance can be the primary source of linearization errors.

(ii) Residual errors left by the linear and nonlinear solvers of the system of reservoir equations

By construction, adjoint-based gradients are the gradients of the sum of the original objective function and a linear combination of the PDE constraints. In theory, the PDE constraints vanish when solving the reservoir equation system. In practice, the residual errors are always present and contribute to the inconsistency between the original objective function value and gradient supplied to the SQP algorithm.

(iii) Different time discretization in different simulations caused by the adaptive time step refinement

Reservoir simulator often employs an adaptive time step refinement algorithm to accurately capture the dynamical behavior of the reservoir. Compressibility, gas or water break-through, and well control updates are phenomena that have a significant impact on the time step size during the adaptive refinement. The refinement algorithm results in a trade-off between accuracy and speed of the simulation. In optimization iterations, any change in the time stepping strategy alters the objective function value.

The first two sources of inconsistency are known and have found remedies in the design of the reservoir simulator and its tuning parameters. The last of the sources has not been studied thoroughly and is the focus of this study.

Errors in the linearization of the model equations can be reduced by using automatic differentiation and smooth nonlinear laws. An automatic differentiation approach allows to avoid the complexity of symbolic manipulations, inaccuracy of numerical differentiation, and effort of finding analytic derivatives. The gradients obtained with automatic differentiation have been successfully used in SQP algorithms to solve PDE constrained optimization problems [9]. This work utilizes automatic differentiation-based general purpose research simulator (AD-GPRS) [26]. AD-GPRS is built on the top of the automatic differentiation expression templates library [31, 35]. This framework is designed to simulate thermal multiphase multi-component flow in porous media [11, 33]. AD-GPRS has several nonlinear formulations [28, 34], generic multi-point flux approximation for space discretization, flexible adaptive implicit method for time discretization [36], and shared-memory parallel

realization [22]. An important part of the AD-GPRS framework is the optimization module [24]. In this module, a general adjoint formulation is used to derive objective gradients for almost any physical reservoir model supported by AD-GPRS.

The inconsistency of the adjoint gradient resulting from residual errors is mitigated by using tight convergence criteria for both linear and nonlinear solvers. It may only slightly increase the time needed for a forward simulation run since a nonlinear solver based on the Newton's method has quadratic convergence near the solution.

The inconsistency of the gradient evaluation as a result of the adaptive time step refinement may be avoided by using a fixed time step discretization for all forward simulations involved in production optimization process. It is achieved by using a dedicated advanced Newton solver, e.g., an adaptively localized continuation method [32] or a trust-region method [27, 30]. These methods guarantee the consistency of the time step refinement from one simulation to another. However, they suffer a large computational burden due to the onerous time step selection algorithm, which is an obstacle for large-scale reservoir simulations.

In this work, we investigate the effects of a typical adaptive time step refinement on the optimization process and optimal solution. In this refinement, the time step selection procedures are limited to the basic instructions, such as prescribing the minimum/maximum time step sizes and increase/decrease factors of the refinement. They are readily available in the majority of reservoir simulators. By varying the degree of time step refinement, we attempt to provide general recommendations for the tuning parameters of the refinement scheme.

In addition, in order to reduce the influence of the time discretization of the simulation on the computation of the objective function, numerical experiments are performed. In these experiments, the objective function is treated as continuous in time and approximated with a high-order numerical integration formula. As a result, a time discretization scheme is obtained and then supplied to the reservoir simulation. In this approach, the commonly used right endpoint rectangle approximation rule is replaced by the Gaussian quadrature rule. We emphasize that the adjoint problem is still managed using the "discretize–then–optimize" approach.

An alternative approach, referred to as "optimize–then–discretize", formulates optimality conditions and an optimization algorithm based on the discrete–in–space and continuous–in–time ordinary differential equation (ODE) form of the problem. An often discussed disadvantage of the "optimize–then–discretize" approach is the inconsistency between the numerical approximation of the continuous gradient and the optimization problem itself, see [10] for a detailed discussion. Here, we mention only that, when time discretizations of the forward and adjoint problems are different, the continuous gradient relies on the accuracy of re-interpolation of the solution of the forward problem, which is beyond the scope of this article. In the case where time discretizations of the forward and adjoint problem coincide, the discrete ODE adjoint systems generated by "optimize–then–discretize" and "discretize–then–optimize" approaches are identical [15].

The well control parameters such as BHP and flow rates are always bounded by the physical limits of the facility equipment and, therefore, explicit nonlinear constraints are common in the production optimization. It is important to investigate the effects of the time step refinement on the nonlinear constraints satisfaction. In our study, two strategies are considered: constraints satisfied during the (i) simulation or (ii) optimization process. In constrained simulation, the violation of a constraint initiates a control switch that may trigger additional changes in the time step refinement. In constrained simulation, the amount by which constraints are violated depends partially on the time step size. Therefore, the time step refinement affects the search for the optimal solution. Previous numerical studies of the SQP algorithm have shown that the optimization with constrained simulation has better performance than constrained optimization [14, 25]. In this work, we use different time step refinement strategies to explain the observed difference.

This paper is organized as follows: the first three sections contain an outline of the adjoint-based gradient algorithm and its application to solving a constrained production optimization problem. The fourth section is devoted to the description of a simple model problem that is employed in all numerical experiments conducted in this work. The main results on the effects of time discretization on the optimization process and its impact on production optimization with nonlinear constraints are presented in Sections 5 and 6. The last section contains conclusions and recommendations.

2 Adjoint-gradient-based production optimization

2.1 Forward simulation

A reservoir is modeled by a system of mass conservation equations

$$\frac{\partial}{\partial t}\left(\phi \sum_p y_{cp}\rho_p s_p\right) + \operatorname{div} \sum_p y_{cp}\rho_p \bar{\mathbf{U}}_p + \sum_p y_{cp}\rho_p \tilde{q}_p = 0, \quad c = 1, \ldots, N_c. \tag{1}$$

Here, we defined

- ϕ – rock porosity
- s_p – mobile phase saturation
- ρ_p – phase molar density
- y_cp – molar fractions
- $\bar{\mathbf{U}}_\mathrm{p}$ – phase velocity
- $\tilde{q}_\mathrm{p}$ – phase volumetric rate per unit bulk volume.

A Darcy's law is used to describe a flux of the phase p

$$\bar{\mathbf{U}}_\mathrm{p} = -\left(\mathbf{k}\frac{k_\mathrm{rp}}{\mu_\mathrm{p}}(\nabla p_\mathrm{p} - \bar{\rho}_\mathrm{p} g \nabla d)\right), \tag{2}$$

where $\mathbf{k}$ and k_rp are absolute and relative permeabilities, μ_p is the viscosity, p_p is the phase pressure, $\bar{\rho}_\mathrm{p}$ is the mass density. In addition, g and d denote the gravitational constant and vertical depth.

To close the system, Eqs. 1–2, we assume instantaneous thermodynamical equilibrium of all components, which can be written as

$$f_{c1}(p, T, \mathbf{y}_1) - f_{cp}(p, T, \mathbf{y}_p) = 0, \tag{3}$$

where $\mathbf{y}_\mathrm{p}$ is the vector of molar fractions and f_cp is the fugacity of the component $c = 1, \ldots, N_\mathrm{c}$ in the phase $p = 1, \ldots, N_\mathrm{p}$.

The reservoir model equations are discretized using a flexible discretization framework [36]. The fully implicit method and two-point flux approximation are applied for the time and space discretizations, respectively. Let $\mathbf{x}_\mathrm{n}$ denote a vector of the state variables (e.g., pressure p, saturation s, and molar fractions y_cp) at time t_n, and $\mathbf{u}_\mathrm{n}$ is the vector of control variables (e.g., target well BHP or phase flow rate) during the time step from t_{n-1} to t_n. This time step size is denoted Δt_n. The notations without subscripts $\mathbf{x}$ and $\mathbf{u}$ are used to describe the full sets of state and control variables taken at all times.

The discretization scheme generates a system of nonlinear algebraic equations

$$\mathbf{g}_\mathrm{n}(\mathbf{x}_\mathrm{n}, \mathbf{x}_{n-1}, \mathbf{u}_\mathrm{n}) = 0. \tag{4}$$

As mentioned previously, the state equation (4) is solved using AD-GPRS. This reservoir simulator admits a generic multi-component multiphase formulation where reduction to a particular physical model (such as black-oil or dead-oil) is obtained as the nonlinear algebraic reduction of the system (1–3). Different combinations of the equations and variables can be employed in AD-GPRS to solve this discrete system of equations [28]. In this work, the natural variable formulation [3, 6] is used where pressure p, saturation s_p and phase concentrations y_cp are defined as nonlinear unknowns for the solution of system (1–3).

After linearization, the resulting system is solved using the generalized minimal residual method (GMRES) with the two-stage constrained pressure residual (CPR) preconditioning [3, 12, 29].

2.2 Optimization problem

The production optimization consists of finding the values of the control variables $\mathbf{u}$ and corresponding values of the state variables $\mathbf{x}$ that maximize the net-present value (NPV) defined by

$$\mathcal{J}(\mathbf{x}, \mathbf{u}) = \sum_{n=1}^{N} \Delta t_n \left(\sum_{j=1}^{N_w}\sum_{p=1}^{N_p} C_{p,j}(t_n) q_{p,j}(\mathbf{x}_n, \mathrm{u}_n)\right), \tag{5}$$

where $q_{p,j}$ and $C_{p,j}$ denote the production/injection phase flow rate and discounted price of the phase p in the j-th well, respectively.

In addition to the objective function (5), the functional specifications of the engineering systems in the reservoir and facilities impose m nonlinear constraints on the state and control variables

$$h_k \leqslant \mathcal{H}_k(\mathbf{x}_\mathrm{n}, \mathbf{u}_\mathrm{n}) \leqslant H_k \quad \forall n = 1, \ldots, N, \tag{6}$$

where $k = 1, \ldots, m$. These inequalities may be either linear with respect to the control variables (e.g., upper and lower bounds on $\mathbf{u}_\mathrm{n}$) or nonlinear (e.g., upper and lower bounds on phase flow rates, gas-oil ratio, or water cut for BHP controlled wells). The intersection of these constraints in the space of pairs $(\mathbf{x}, \mathbf{u})$ defines a feasibility region of the production optimization problem, denoted here as D.

Using Eqs. 4–6, the production optimization problem can be stated as

$$\underset{\mathbf{x},\mathbf{u}}{\text{maximize}} \quad \mathcal{J}(\mathbf{x}, \mathbf{u}), \tag{7a}$$

$$\text{subject to} \quad \mathbf{g}_\mathrm{n}(\mathbf{x}_\mathrm{n}, \mathbf{x}_{n-1}, \mathbf{u}_\mathrm{n}) = 0, \tag{7b}$$

$$\mathbf{x}_0 = x(t_0), \tag{7c}$$

$$(\mathbf{x}, \mathbf{u}) \in D. \tag{7d}$$

The state variables $\mathbf{x}$ appear as unknowns in the optimization problem (7a–7d). However, because their number corresponds to the number of equations in Eq. 7b, they can be efficiently eliminated from $\mathcal{J}$ and $\mathcal{H}_k$ to reduce the computational load of the SQP algorithm. We notice that, although, the SQP implementation used in this work is designed for problems with many thousands of constraints and variables, this implementation is best suited for problems with up to 2000 degrees of freedom [8]. The next section describes the adjoint algorithm applied to eliminate the state variables.

2.3 Adjoint algorithm

The most efficient way to eliminate $\mathbf{x}$ from Eq. 7a is an application of the adjoint variable method. In this method, one constructs a Lagrangian function $\mathcal{L}$ which effectively

replaces the original objective function $\mathcal{J}$ in such a way that, once Eq. 7b is satisfied, $\mathcal{L}$ would have the same critical points (i.e., points where the gradient is zero) as $\mathcal{J}$. By construction

$$\mathcal{L} = \mathcal{J} + \sum_{n=1}^{N} \boldsymbol{\lambda}_{\mathrm{n}}^{T} \mathbf{g}_{\mathrm{n}}(\mathbf{x}_{\mathrm{n}}, \mathbf{x}_{n-1}, \mathbf{u}_{\mathrm{n}}), \tag{8}$$

where $\boldsymbol{\lambda}_{\mathrm{n}}^{T}$ is a Lagrange multiplier corresponding to the state equation $\mathbf{g}_{\mathrm{n}}$. An extremum of the Lagrangian (8), with respect to $\mathbf{x}$, $\mathbf{u}$, and $\boldsymbol{\lambda}$, is located either at a critical point or on the boundary of the feasibility region D.

Let us postpone the feasibility discussion until the next section and just consider the algorithm for searching critical points. By setting the total variation of the Lagrangian to zero, a system of equations called the first optimality conditions is obtained, see [18]

$$\mathbf{g}_{\mathrm{n}}(\mathbf{x}_{\mathrm{n}}, \mathbf{x}_{n-1}, \mathbf{u}_{\mathrm{n}}) = 0, \tag{9a}$$

$$\left(\frac{\partial \mathbf{g}_{\mathrm{n}}}{\partial \mathbf{x}_{\mathrm{n}}}\right)^{T} \boldsymbol{\lambda}_{\mathrm{n}} + \left(\frac{\partial \mathbf{g}_{n+1}}{\partial \mathbf{x}_{\mathrm{n}}}\right)^{T} \boldsymbol{\lambda}_{n+1} + \left(\frac{\partial \mathcal{J}}{\partial \mathbf{x}_{\mathrm{n}}}\right)^{T} = 0, \tag{9b}$$

$$\left(\frac{\partial \mathbf{g}_{\mathrm{n}}}{\partial \mathbf{u}_{\mathrm{n}}}\right)^{T} \boldsymbol{\lambda}_{\mathrm{n}} + \left(\frac{\partial \mathcal{J}}{\partial \mathbf{u}_{\mathrm{n}}}\right)^{T} = 0, \tag{9c}$$

for $n = 1, 2, \ldots, N$. Equations 9b are adjoint equations based on the transposed Jacobian matrix from Eq. 9a. They are solved backward-in-time and, therefore, supplied with a fictitious initial condition

$$\boldsymbol{\lambda}_{N+1} = 0, \tag{10}$$

to satisfy Eq. 9b for $n = N$ [15].

Equations 9a and 9b are used to compute state $\mathbf{x}$ and adjoint $\boldsymbol{\lambda}$ variables, respectively. The third condition Eq. 9c is utilized to define the total variation of the objective function $\mathcal{J}$, corresponding to an arbitrary perturbation of the control variables $\delta\mathbf{u}_{\mathrm{n}}$

$$d\mathcal{J} = d\mathcal{L} = \sum_{n=1}^{N} \left[\boldsymbol{\lambda}_{\mathrm{n}}^{T} \frac{\partial \mathbf{g}_{\mathrm{n}}}{\partial \mathbf{u}_{\mathrm{n}}} + \frac{\partial \mathcal{J}}{\partial \mathbf{u}_{\mathrm{n}}}\right] \delta\mathbf{u}_{\mathrm{n}}. \tag{11}$$

The square bracket term in Eq. 11 does not depend on the perturbation $\delta\mathbf{u}_{\mathrm{n}}$. In the space of controls $\mathbf{u}_n$, it is a vector orthogonal to the level sets of $\mathcal{J}$ pointing in the direction of the steepest increase of $\mathcal{J}$. This row-vector term is called the adjoint-based gradient and denoted by $\nabla_{\mathbf{u}_{\mathrm{n}}}\mathcal{J}$. The gradient thus obtained is supplied to the SQP algorithm and constructs the approximation of Hessian and quadratic model of $\mathcal{J}$ using a variation of the Broyden-Fletcher-Goldfarb-Shanno (BFGS) algorithm. A detailed description of the SQP algorithm is provided in [8].

So far, $\mathbf{u}$ has been considered to vary over the same time steps as $\mathbf{x}$. However, well control parameters (such as BHP or phase flow rates) are usually discretized on a time scale coarser than the time steps of the reservoir simulation. This coarse time-scale is called the control steps further in the paper. It can be readily shown that the gradient corresponding to a control step is a sum of the gradient terms computed for each time step in this control step. For example, if the time steps $\{n_i, n_i+1, \ldots, n_{i+1}-1\}$ belong to the i-th control step, the gradient of an objective function with respect to the i-th control variable $\mathbf{U}_i$ ($\mathbf{U}$ denotes the vector control variables discretized at control steps) is defined as

$$\nabla_{\mathbf{U}_i}\mathcal{J} = \sum_{n=n_i}^{n_{i+1}-1} \left[\boldsymbol{\lambda}_n^{T} \frac{\partial \mathbf{g}_n}{\partial \mathbf{u}_n} + \frac{\partial \mathcal{J}}{\partial \mathbf{u}_n}\right]. \tag{12}$$

The adjoint-based gradient algorithm is also applied to linearize constraint functions utilized in the SQP algorithm. This procedure is explained in the next section.

3 Nonlinear constraints

In this paper, the focus is on nonlinear constraints corresponding to the well characteristics that may, otherwise, be employed as well control parameters. For example, constraints on the well phase flow rates are frequently applied as controls in the reservoir simulations. The well characteristics that do not satisfy this criterion are, for example, the water cut and gas-oil ratio.

As mentioned previously, in the constrained optimization problem (7a–7d), some control variables do not have to satisfy $\nabla_{\mathbf{U}_i}\mathcal{J} = 0$ once they attain the boundary of the feasibility region D. Two strategies to handle those variables are considered: (i) constraints in reservoir simulation and (ii) nonlinear constraints in the optimization problem.

3.1 Constraints in reservoir simulation

In this strategy, the production optimization problem (7) is simplified to Eqs. 7a, 7b, 7c and upper/lower bounds of $\mathbf{u}$. Nonlinear constraints from Eq. 7d are satisfied immediately during simulation (see [7, 26] for details) in the following way. Each well is supplied with a default control and constraints. When a constraint cannot be satisfied in a particular time step, it switches the role with the control. The rules for switching are directly implemented in the nonlinear solver of a reservoir simulator. The main disadvantage of this strategy is that, when switching occurs, the sensitivity of $\mathcal{J}$ with respect to the default well control is not computed. At the same time, the variables of the production optimization problem are always associated with the target values of the default well control parameters. Therefore, if control switch occurs at every time step of a control step, the adjoint gradient term corresponding to this control step vanishes. The optimization variables corresponding to the vanishing gradient terms hold their current values till the end of the

optimization iteration. Accurate estimation of the sensitivity as a result of a control switch and its effect on the optimal solution is a separate topic and will be discussed in future work.

3.2 Constraints in optimization problem

In this strategy, a quadratic model of the objective function is supplemented with linear models of the constraint functions (6). The linearization of the constraints Eq. 6 is done using an adjoint variable algorithm similar to the one described in Section 2.3. The sensitivities with respect to the control variables have the form

$$\nabla_{\mathbf{U}_i}\mathcal{H}_k = \sum_{n=n_i}^{n_{i+1}-1}\left[\boldsymbol{\mu}_{k,n}^T\frac{\partial \mathbf{g}_n}{\partial \mathbf{u}_n} + \frac{\partial \mathcal{H}_k}{\partial \mathbf{u}_n}\right], \tag{13}$$

where $k = 1, \ldots, m$ and $\boldsymbol{\mu}_{k,n}$ are the adjoint variables of $\mathcal{H}_k(\mathbf{x}, \mathbf{u})$ satisfying

$$\left(\frac{\partial \mathbf{g}_n}{\partial \mathbf{x}_n}\right)^T\boldsymbol{\mu}_{k,n} + \left(\frac{\partial \mathbf{g}_{n+1}}{\partial \mathbf{x}_n}\right)^T\boldsymbol{\mu}_{k,n+1} + \left(\frac{\partial \mathcal{H}_k}{\partial \mathbf{x}_n}\right)^T = 0, \tag{14a}$$

$$\boldsymbol{\mu}_{k,N+1} = 0. \tag{14b}$$

We emphasize that the transposed Jacobian matrix $(\partial \mathbf{g}_n / \partial \mathbf{x}_n)^T$ used in Eq. 14a is identical to the one introduced in Eq. 9b. In practice, the matrix $(\partial \mathbf{g}_n / \partial \mathbf{x}_n)^T$ is constructed once and utilized for $\boldsymbol{\lambda}_n$ and $\boldsymbol{\mu}_{k,n}$. Therefore, a single backward simulation is performed which requires, at each time step, to solve $1 + m$ linear systems. In large production optimization problems, this approach is more efficient than running multiple backward simulations, i.e., one for the objective function, and one for each constraint.

A quadratic model of $\mathcal{J}$ is constructed and solved as a QP sub-problem

$$\begin{aligned}\underset{\xi}{\text{maximize}}\ & \mathcal{J}^{(l)} + \nabla_{\mathbf{U}}\mathcal{J}^{(l)}\left(\xi - \mathbf{U}^{(l)}\right)\\ & + \tfrac{1}{2}\left(\xi - \mathbf{U}^{(l)}\right)^T\nabla^2_{\mathbf{U}}\mathcal{J}^{(l)}\left(\xi - \mathbf{U}^{(l)}\right),\\ \text{subject to}\ & h_k \leqslant \mathcal{H}_k^{(l)} + \nabla_{\mathbf{U}}\mathcal{H}_k^{(l)}\left(\xi - \mathbf{U}^{(l)}\right) \leqslant H_k,\end{aligned} \tag{15}$$

where $k = 1, \ldots, m$, $\nabla^2_{\mathbf{U}}\mathcal{J}^{(l)}$ is an approximation of the Hessian and l corresponds to the current optimization iteration. The optimal solution of Eq. 15 contributes to the search direction of the next update of $\mathbf{U}$.

In the constrained optimization strategy, all underlying simulations are unconstrained which has one positive and one negative implication. On the positive side, the control switch is not triggered, and the sensitivity of $\mathcal{J}$ is not missing which allows a broad exploration of the control space. On the negative side, the truncation error introduced by linearization of the nonlinear constraints requires frequent updates of the gradient that may significantly slow down the optimization process.

Linearization requires a constraint function $\mathcal{H}_k$ to be differentiable. However, after being lumped in time, the upper and lower bound constraints on the well flow rate become obviously non-differentiable

$$\mathcal{H}_k(\mathbf{x}_\mathrm{n}, \mathbf{u}_\mathrm{n}) \leqslant H_k\ \forall n \ \Leftrightarrow\ \max_\mathrm{n}\mathcal{H}_k(\mathbf{x}_\mathrm{n}, \mathbf{u}_\mathrm{n}) \leqslant H_k, \tag{16a}$$

$$h_k \leqslant \mathcal{H}_k(\mathbf{x}_\mathrm{n}, \mathbf{u}_\mathrm{n})\ \forall n \ \Leftrightarrow\ h_k \leqslant \min_\mathrm{n}\mathcal{H}_k(\mathbf{x}_\mathrm{n}, \mathbf{u}_\mathrm{n}). \tag{16b}$$

A smooth approximation of the maximum and minimum functions is utilized and defined as follows

$$\max(a, b) \cong \frac{a + b + \sqrt{(b-a)(b-a) + \varepsilon}}{2}, \tag{17a}$$

$$\min(a, b) \cong \frac{a + b - \sqrt{(b-a)(b-a) + \varepsilon}}{2}, \tag{17b}$$

where ε is the parameter that ensures smoothness of the derivative. If the values of a and b are smaller than one, ε needs to be scaled down to maintain the accuracy of the approximation. In the production optimization, meaningful a and b are often larger than one and we can assign $\varepsilon = 10^{-10}$ with a view to prevent the square root in Eqs. 17a and 17b from vanishing. The approximation (17) seems to be particularly suitable for the production optimization (refer to Appendix A).

The approximation (17) is applied recursively, in conjunction with automatic differentiation, to evaluate $\max_\mathrm{n}\mathcal{H}_k(\mathbf{x}_\mathrm{n}, \mathbf{u}_\mathrm{n})$, $\min_\mathrm{n}\mathcal{H}_k(\mathbf{x}_\mathrm{n}, \mathbf{u}_\mathrm{n})$ and their partial derivatives with respect to $\mathbf{x}_\mathrm{n}$ and $\mathbf{u}_\mathrm{n}$ employed in Eqs. 13 and 14a.

3.3 SQP algorithm

The optimization problem is solved using the SQP code implemented in the sparse nonlinear optimizer (SNOPT) library. A detailed description of this library can be found in [8]. SNOPT is coupled with the AD-GPRS sub-routines calculating the gradients of the objective function and nonlinear constraints. The optimization iterations loop consists of the following steps

Algorithm 1

$l \leftarrow 0$
$\mathbf{U}^{(0)} \leftarrow$ initial guess
repeat
  given estimate of $\mathbf{U}^{(l)}$, solve (9a) for $\mathbf{x}^{(l)}$
  given $\mathbf{x}^{(l)}$ and $\mathbf{U}^{(l)}$, solve (9b) for $\lambda^{(l)}$
  update the gradient $\nabla_\mathrm{U} J^{(l)}$ and Jacobian $\nabla_\mathrm{U} H_k^{(l)}$
  solve QP problem (15) to find the search direction
  perform a line search to find a new estimate $\mathbf{U}^{(l+1)}$
  $l \leftarrow l + 1$
until termination criteria are satisfied.

A sequence of optimization solutions $\mathbf{U}^{(l)}$ is considered converged when the KKT conditions described in [8] are satisfied to a given tolerance.

4 Case study

For all studies below, a standard water flooding model with a complex geology and simplified physical properties is considered. The model includes a reservoir of dimensions $30 \times 110 \times 10$ described by layers 33 to 42 of the upscaled SPE10 model [5]. The logarithm of permeability of this model and the initial oil saturation are shown in Fig. 1.

The reservoir is supplied with nine vertical water injection wells (W1, W2, W3, W6, W7, W8, W11, W12, W13) and four vertical producers (W4, W5, W9, W10) completed through all ten layers. The base case, which is also an initial guess for the optimization, uses control targets such that the well BHPs are 300 bars for producers and 500 bars for injectors. The physical properties of both fluid and rock are taken from [23] and summarized in Table 1:

In this study, two types of NPV are considered:

- *without water penalty* (i.e., water production and injection costs are zero)
- *with a large water penalty* (i.e., water production and injection costs are set to 6 \$/bbl)

The oil production price is 75 \$/bbl. The water cost is added to avoid the trivial solution of the full blast when no nonlinear constraints are present. This work focuses on the short-term production optimization where the NPV behavior is dictated by the oil production term. In all cases below, the optimization process is terminated when the KKT conditions described in [8] are satisfied to a given tolerance, or the number of gradient evaluations exceeds 60.

Table 1 Parameter values for models

Parameter	Value	Description
ϕ	20 %	Porosity
c_r	10^{-5} 1/bar	Rock compressibility
c_o, c_w	10^{-5} 1/bar	Fluid compressibility
ρ_o, ρ_w	1000 kg/m^3	Fluid density
μ_o, μ_w	1 cP	Fluid viscosity
$S_{w,ini}$	0.1	Initial water saturation
S_{wr}, S_{or}	0	Rel. perm. endpoints
n_w, n_o	2	Rel. perm. exponents

5 Time step refinement and optimization process

An iterative optimization algorithm often requires multiple evaluations of the objective function. Therefore, a reservoir simulation performed at each evaluation should be accomplished in a reasonable amount of time. For this purpose, one often employs the fully implicit first-order discretization schemes with a reasonable large time step. Although this may not be an issue in the reservoir simulation, it may affect the value of the objective function in production optimization. This claim is investigated by an example of the unconstrained production optimization with a large water penalty, based on a test model presented earlier.

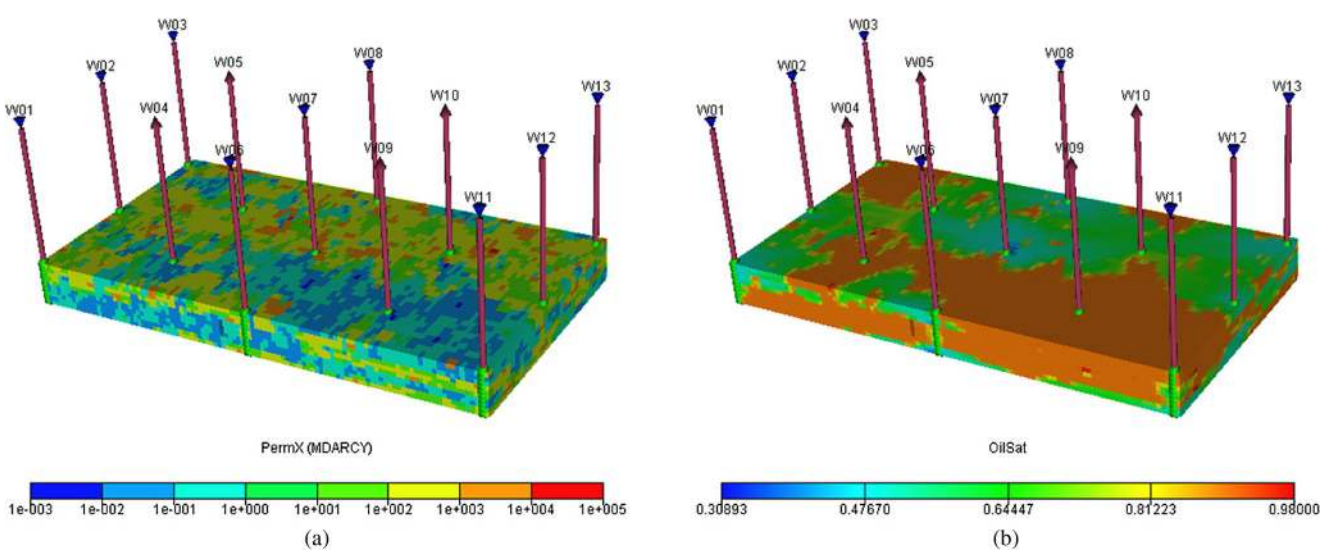

Fig. 1 Logarithm of permeabilities (**a**) and base case oil saturation (**b**) for Example 2

5.1 The influence of the time step refinement on the computation of NPV

This section investigates the response of the objective function to the time step refinement in reservoir simulation with fixed control variables corresponding to the initial guess. Six simulations are performed, each with constant time steps of $\Delta t = 1, 2, 4, 8, 16$, and 32 days. All simulations contain six control steps of 32 days each. Figure 2 shows the change of the NPV as a function of time step size. In Fig. 2, three curves in each plot match three control scenarios:

Case 1. BHP controlled production and injection,
Case 2. BHP controlled production and rate controlled injection,
Case 3. Rate controlled production and BHP controlled injection.

Nonlinear regression of the NPV values with the function Δt^{α} gives $\alpha = 1.012, 0.963, 1.028$ for Cases 1, 2, and 3, respectively. Although NPV changes linearly with respect to the time step size Δt, this change has a different origin in Case 3 versus Cases 1 and 2. In Cases 1 and 2, the large variation is observed in the oil production term, which is the major contributor to the NPV. In Case 3, the oil production term does not change with Δt, and the change of the NPV as function of Δt is generated by minor contributors, i.e., water production and injection terms. The large variation non-controlled production/injection rates can occur as a result of:

- numerical integration error in the computation of the NPV function,
- accumulation of phase rate evaluation errors for well BHP being a control parameter.

We denote by $t_1, \ldots, t_N$ an initial discretization used in the example problem. To mitigate the integration error, the NPV function is redefined using a high-order numerical integration described below.

The production optimization problem is reformulated, with the objective function $\mathcal{J}$ in Eq. 5 replaced by the sum of integrals

$$\widetilde{\mathcal{J}} = \sum_{n=1}^{N} \int_{t_n}^{t_{n+1}} \left(\sum_{j=1}^{N_w} \sum_{p=1}^{N_p} C_{p,j} q_{p,j} \right) dt, \tag{18}$$

where t_n and t_{n+1} are the start and end points of the n-th time step. $C_{p,j}\, q_{p,j}$ is considered to be a continuous function of time, with the sum of integrals in Eq. 18 approximated by a

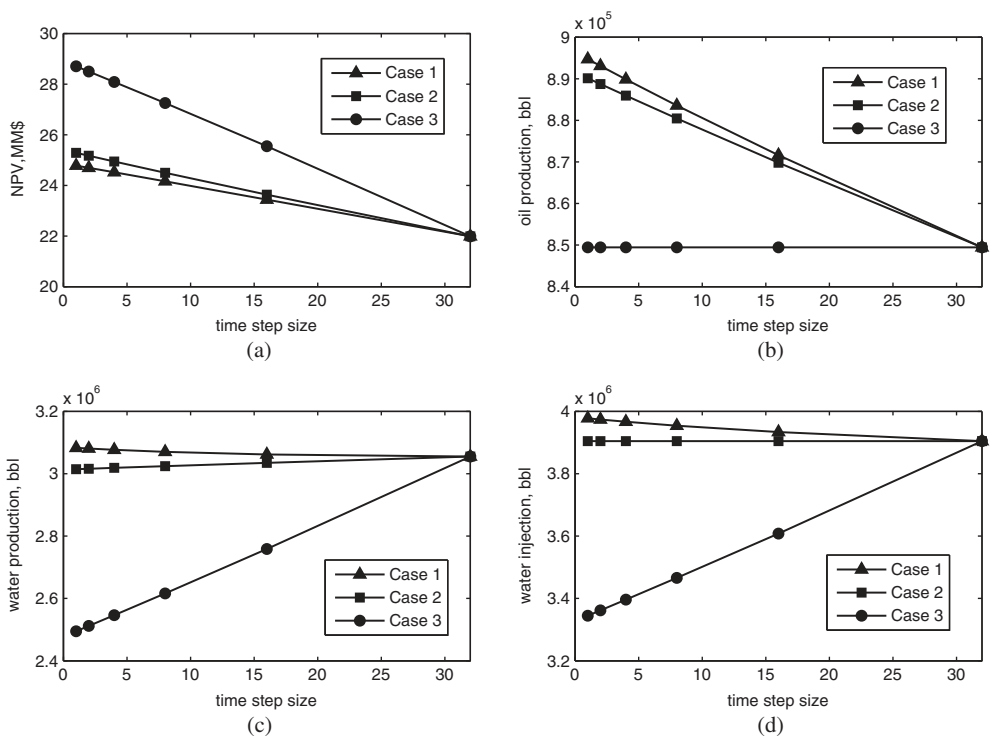

Fig. 2 Cumulative **a** NPV, **b** oil production, **c** water production, **d** water injection after 192 days as a function of the time steps size used in the underlying reservoir simulations. Each simulation is performed at fixed control variables corresponding to the initial guess with constant time steps of $\Delta t = 1, 2, 4, 8, 16$, and 32 days

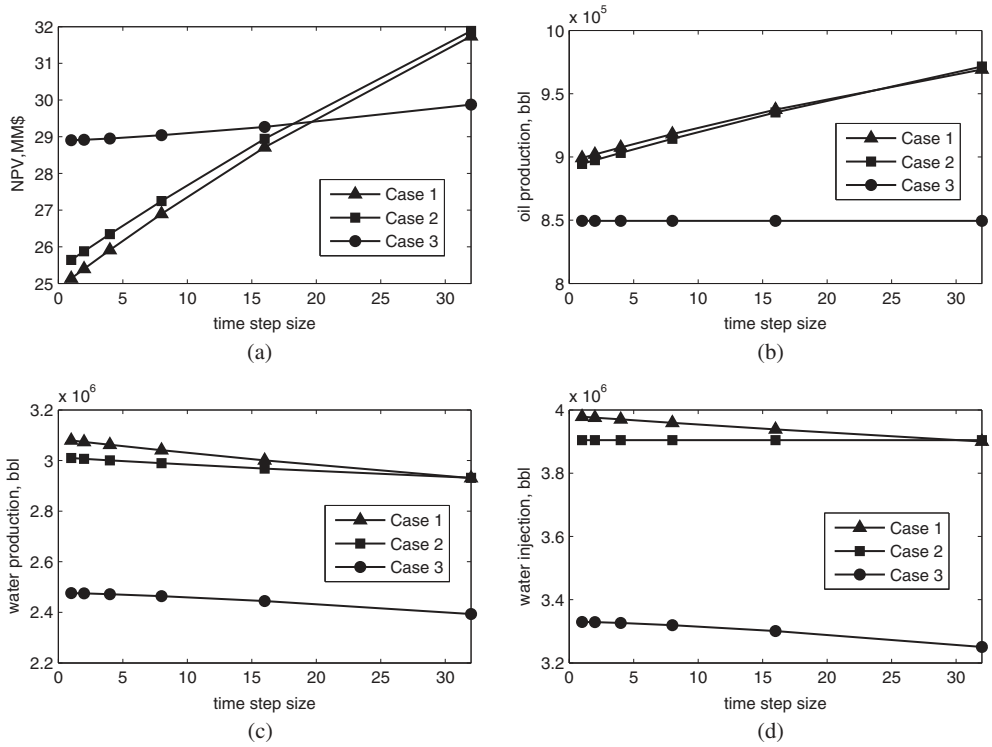

Fig. 3 Cumulative **a** NPV, **b** oil production, **c** water production, and **d** water injection, corresponding to the second-order integration formula (19). Each simulation is performed at fixed control variables corresponding to the initial guess with the time step refinement defined by constant time steps of $\Delta t = 1, 2, 4, 8, 16$, and 32 days, and supplemented with Gauss quadrature points

composite Gaussian quadrature formulas [21], resulting in a discrete form of $\widetilde{\mathcal{J}}$

$$\mathcal{J}_g = \sum_{n=1}^{N} \sum_{r=1}^{N_g} \frac{\Delta t}{2} W_r \left(\sum_{j=1}^{N_w} \sum_{p=1}^{N_p} C_{p,j} q_{p,j} \right) \Bigg|_{t=\tau_{n,r}}, \qquad (19)$$

where $\tau_{n,r} = 1/2\,(t_n + t_{n+1}) + 1/2\,\Delta t\,\xi_r$. ξ_r are the quadrature points in $(-1, 1)$ and W_r are the associated weights for $r = 1, \ldots, N_g$. Next,

$$t_1, \tau_{1,1}, \ldots, \tau_{1,N_g}, t_2, \tau_{2,1}, \ldots, \tau_{2,N_g}, \ldots, t_N, \tau_{N,1}, \ldots, \tau_{N,N_g}$$

is designated as the time discretization points in the reservoir simulation and the optimization problem (17) is solved with the objective function $\mathcal{J}$ replaced by $\mathcal{J}_g$, defined in Eq. 19. It is shown in [21] that for a constant step Δt the numerical integration error is of the order $O(\Delta t^{2N_g})$.

Figure 3 shows a change of the objective function $\mathcal{J}_g$ with respect to the time step size for $N_g = 1$. One notices that Cases 1 and 2 exhibit a considerable change in $\mathcal{J}_g$ and the corresponding cumulative oil production. At the same time, in Case 3, the change in $\mathcal{J}_g$ is less prominent than the change

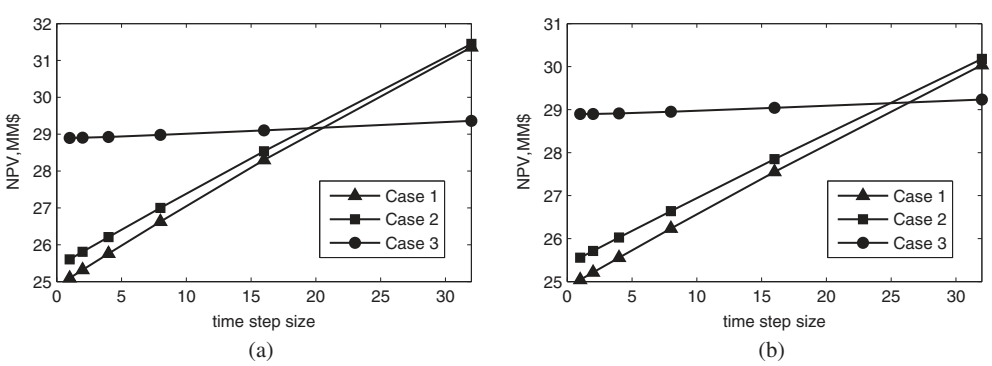

Fig. 4 Cumulative NPV corresponding to the **a** third- and **b** fourth-order integration formula (19). Each simulation is performed at fixed control variables corresponding to the initial guess, with the time step refinement defined by constant time steps of $\Delta t = 1, 2, 4, 8, 16$, and 32 days, and supplemented with Gauss quadrature points

in the original NPV depicted in Fig. 2. The conclusion in Case 3 is that the variation of the original NPV, defined in Eq. 5, is a result of the numerical integration error in the computation of the NPV function. Whereas, in Cases 1 and 2, it is due to the accumulation of phase rate evaluation errors. The behavior of Cases 1, 2, and 3 is confirmed in Fig. 4 for high-order Gauss quadrature formulas $N_g = 2$ and 3.

We conclude that the variation of the NPV, with respect to the time step size, has to be taken into account in the optimization process and analysis of the optimal solution. In the case of production optimization with well BHP control variables, the differences in the time discretization generate an accumulation of phase rate evaluation errors that make objective function evaluation inconsistent between different simulation runs. This inconsistency is passed onto the SQP algorithm and affects line search, adjoint gradients, and approximation of the Hessian. Our recommendation is that the results of the case studies in production optimization, in particular with BHP controls, should be accompanied by a test of robustness with respect to time step refinement.

5.2 The influence of the time step refinement on the optimal solution

Next, the focus is on the consistency of optimal solutions obtained with reservoir simulations, subject to time step refinements $\Delta t = 1, 2, 4, 8, 16$, and 32 days, introduced previously. Figure 5 illustrates the correlation of optimization variables $\mathbf{U}^{(l)}$ corresponding to $\Delta t = 1, 2, 4, 8, 16$, and 32 days, as they progress through optimization iteration $l = 10$, 20, and 40. The correlation is calculated by

$$\mathrm{corr}(\mathbf{U}_\alpha^{(l)}, \mathbf{U}_\beta^{(l)}) = \frac{\left\langle \mathbf{U}_\alpha^{(l)} - \overline{\mathbf{U}_\alpha^{(l)}}, \mathbf{U}_\beta^{(l)} - \overline{\mathbf{U}_\beta^{(l)}} \right\rangle}{||\mathbf{U}_\alpha^{(l)} - \overline{\mathbf{U}_\alpha^{(l)}}||\,||\mathbf{U}_\beta^{(l)} - \overline{\mathbf{U}_\beta^{(l)}}||}, \tag{20}$$

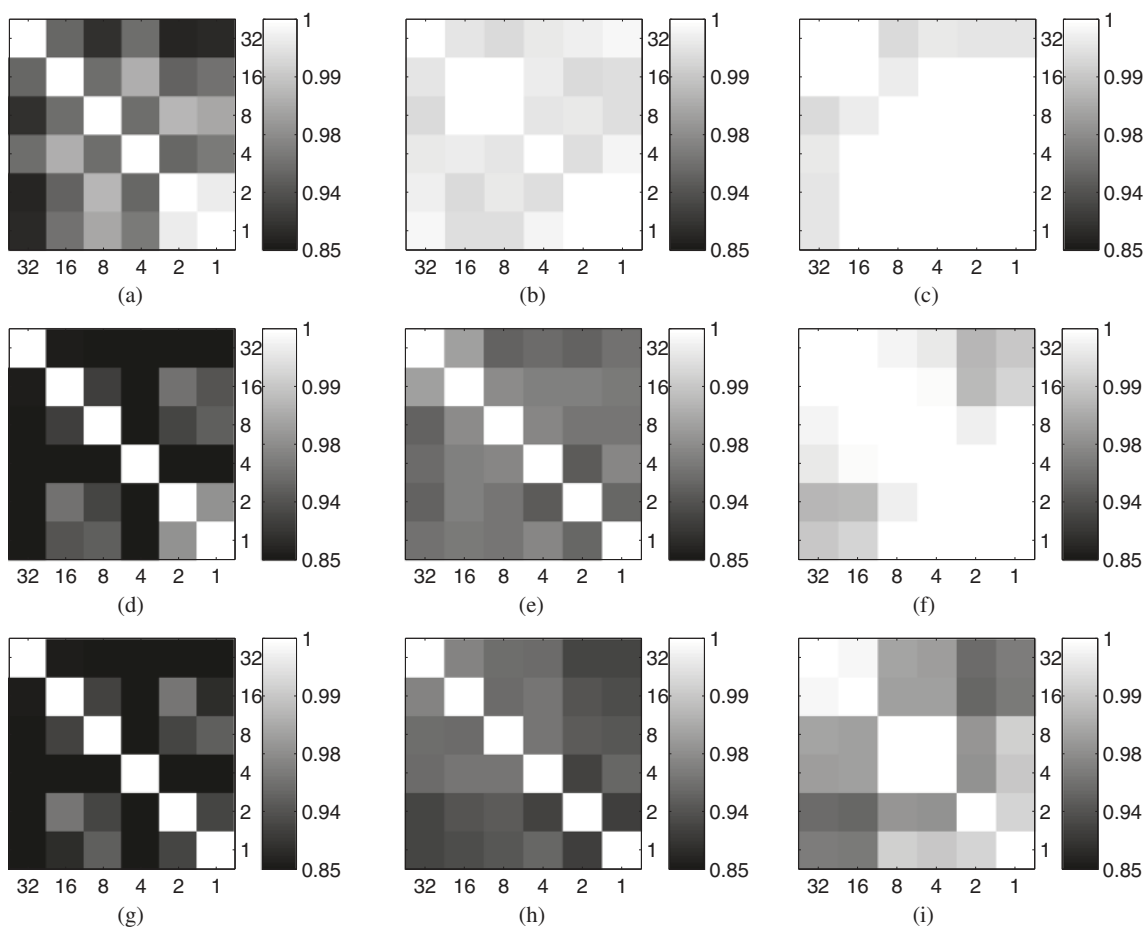

Fig. 5 Correlation of the optimization variables obtained when using reservoir simulations with constant time steps $\Delta t = 1, 2, 4, 8, 16$, and 32 days, at optimization iterations **a, b, c** $l = 10$, **d, e, f** $l = 20$, and **g, h, i** $l = 40$. Here, **a, d, g** correspond with Case 1, **b, e, h** with Case 2, and **c, f, i** with Case 3

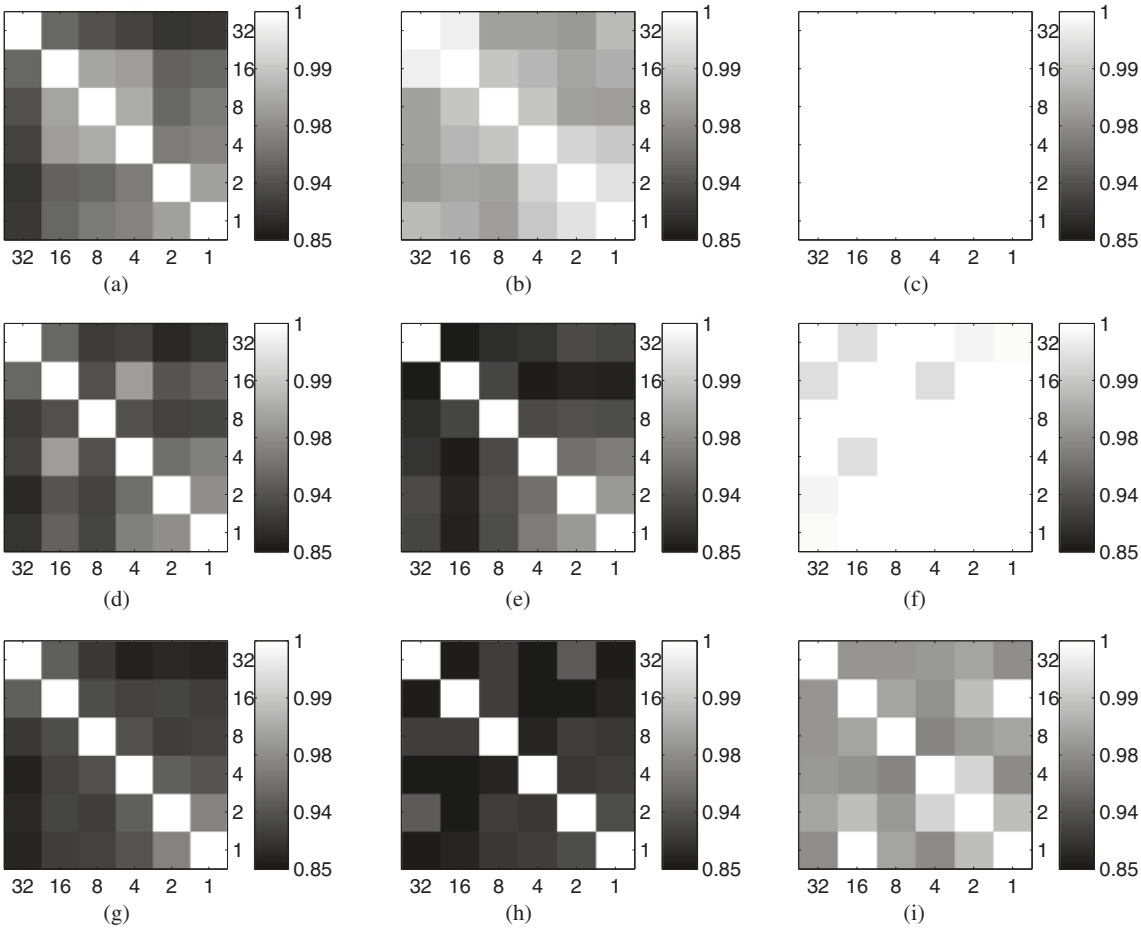

Fig. 6 Correlation of the optimization variables obtained when using reservoir simulations with the time step refinement defined by constant time steps of $\Delta t = 1, 2, 4, 8, 16$, and 32 days and supplemented with Gauss quadrature points. The optimal variables are compared at the optimization iterations **a, b, c** $l = 10$, **d, e, f** $l = 20$, and **g, h, i** $l = 40$ for **a, d, g** Case 1, **b, e, h** Case 2, and **c, f, i** Case 3

where $\mathbf{U}_{\alpha}^{(l)} = \mathbf{U}^{(l)}|_{\Delta t=\alpha}$ for $\alpha, \beta \in 1, 2, 4, 8, 16$, and 32 days.

In Case 1, all solutions $\mathbf{U}^{(l)}$ except those corresponding to $\Delta t = 1$ and 2 deviate largely at $l = 10$, see Fig. 5a. By the 40th iteration, their correlation decreases further to 83 ± 13 %, see Fig. 5g. In Case 2, the solutions $\mathbf{U}^{(l)}$ have a high correlation at $l = 10$, see Fig. 5b, which becomes 94 ± 2 % at $l = 40$, see Fig. 5h. In Case 3, the solutions $\mathbf{U}^{(l)}$ remain highly correlated for $l = 10$ through 20, see Fig. 5c, f. As the optimal solution is approached at $l = 40$,

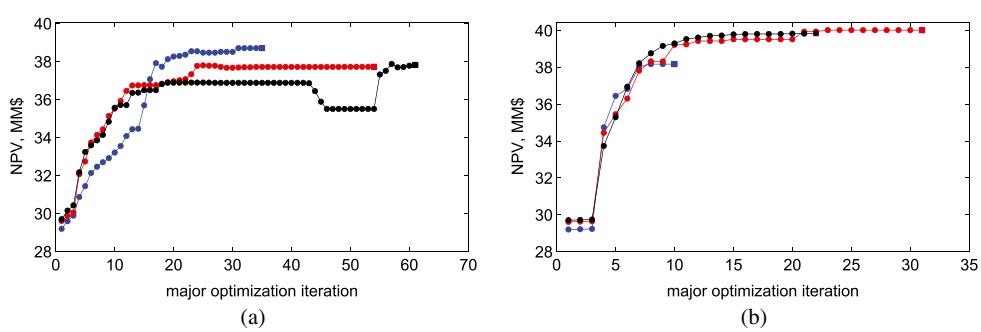

Fig. 7 NPV as a function of major optimization iterations for **a** constrained optimization and **b** optimization with constrained simulations; all simulations performed for small (*black*), medium (*red*), and large (*blue*) time step refinements after control update

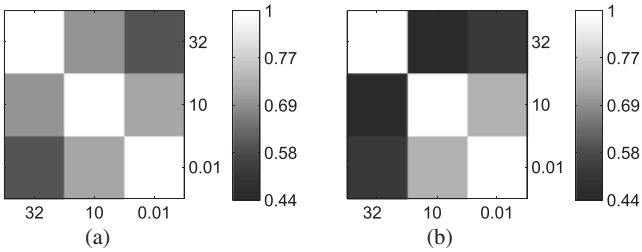

Fig. 8 Correlation of the optimal solution computed using small, medium, and large refinement scenarios for **a** constrained optimization and **b** optimization with constrained simulations

the correlation of Case 3 slightly decreases to 98 ± 2 %, due to the time truncation errors in forward simulations, see Fig. 5i.

Similar results are observed for $\mathcal{J}_g$, i.e., when the original NPV function (5) is replaced with the second-order numerical integration formula (19) with $N_g = 1$, see Fig. 6.

We conclude that the significant variation of correlations among Cases 1, 2, and 3 in Figs. 5 and 6 is attributed to the differences in phase rate evaluations of the oil production of BHP controlled wells. We recall that this study was performed using reservoir simulations with constant time steps. In practice, however, the time step size varies through the control step. Often, the decrease in the time step size occurring after the control update has a particular implication in the case of the constrained production optimization.

6 Time step refinement and nonlinear constraints

In the previous section, we investigated well control scenarios corresponding to an unconstrained optimization problem. Constraints introduce additional complexity resulting from the change of the well equation when switching controls from BHP to phase rate and vice versa. Here, we consider a production optimization problem without water penalty. In this formulation and specifically for incompressible two-phase problems, the NPV is proportional to the water injection rate. The main purpose of this simplification is to make production optimization problems convenient for systematic analysis.

This study focuses on BHP controlled production and injection, i.e., Case 1 in Section 5. As stated above, this control scenario admits large changes in oil production for time steps varying from 1 to 32 days. To isolate the effects of the adaptive time refinement, the production BHP controls are fixed to the initial values. In such case, the optimization variables are the target values of the injection BHP with upper-bound constraints on the injection flow rates.

According to theory [17], an instantaneous change of the BHP value results in a singularity of the phase flow rate. If the BHP control remains constant for a long period afterward, the corresponding phase flow rate converges asymptotically to a constant value. In the numerical simulation, the sizes of the control step and the first time step after control update are finite. Therefore, the singularity turns into an instantaneous increase/decrease of the phase flow

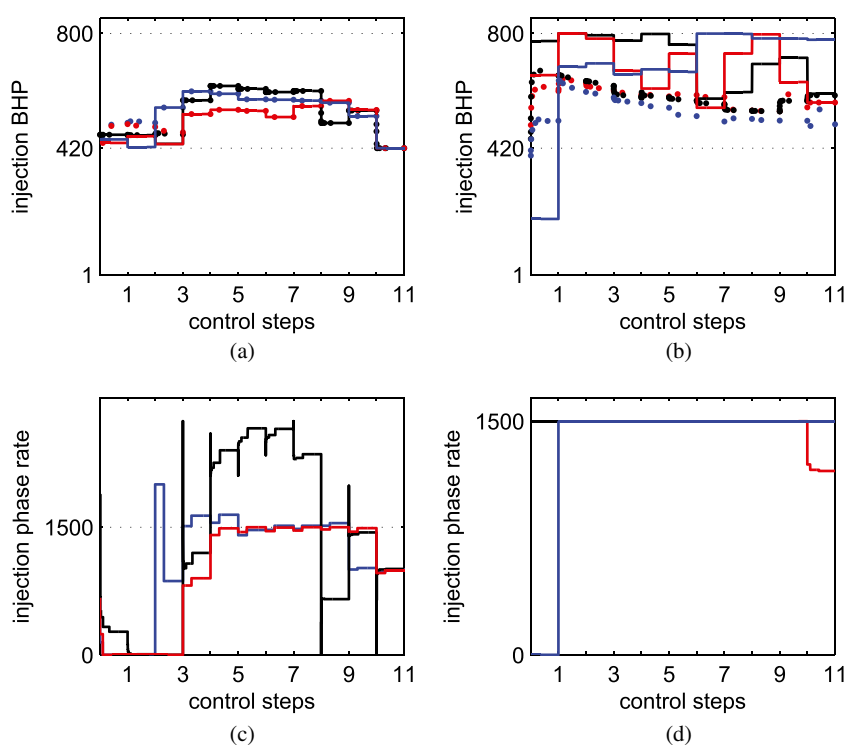

Fig. 9 Injection BHP and phase flow rates of well W07 for constrained optimization (**a,c**) and optimization with constrained simulations (**b,d**); all simulations performed for small (*black*), medium (*red*) and large (*blue*) time step refinements after control update

rate value followed by the rate adjustment. The magnitude of the pick and duration of the adjustment period depend on the reservoir properties, as well as on the size of the first time step after control update. In a reservoir simulation, the adjustment period is often smaller than a typical time step size that does not affect results. However, an extremely fine time step after control update may reveal the pick and trigger the rate constraint violation.

The effects of time step refinement are studied for two implementations of the nonlinear constraints: (i) optimization with constrained simulations and (ii) constrained optimization. We use the setup of Section 5 and replace the constant time steps with three patterns of the refinement: small, medium, and large. For small refinement, the highest time step after control update is 0.01 day, for medium — 10 days, and for large — 32 days (meaning no refinement). Afterward, the time step size is gradually increased by a factor of three until it reaches the next control step. Time step adjustment with respect to changes in state variables $\mathbf{x}$ is not applied in this strategy. The production optimization is performed on 11 control steps of 32 days each. The upper bound constraint of injection wells is 1500 m^3/day.

Figure 7 shows a comparison of the NPV for the cases of optimization with constrained simulation and constrained optimization. Here, the final values of the NPV are traced at the major optimization iterations (i.e., evaluations of the adjoint gradient) for small (black), medium (red), and large (blue) time step refinements. Next, those results are used to analyze various aspects of the optimization process.

6.1 Robustness with respect to the time step refinement

One notices that the final values of the NPV for the small and medium refinements are similar (black and red lines, respectively) in both constraining strategies. On the contrary, the values for the large refinement (blue line) differ from others quantitatively, as well as qualitatively. For constrained optimization, the large refinement performed better than the small and medium ones, whereas it failed for optimization with constrained simulations. This behavior is analyzed later. Here, the focus is on the robustness of the optimal solution. Similar to the case of unconstrained production optimization presented earlier, constrained optimization in Fig. 7 clearly demonstrates robustness with respect to the time step refinement. The correlations of the optimal solution, computed using Eq. 20, give 65 ± 5 % for constrained optimization and 58 ± 15 % for optimization with constrained simulations, see Fig. 8.

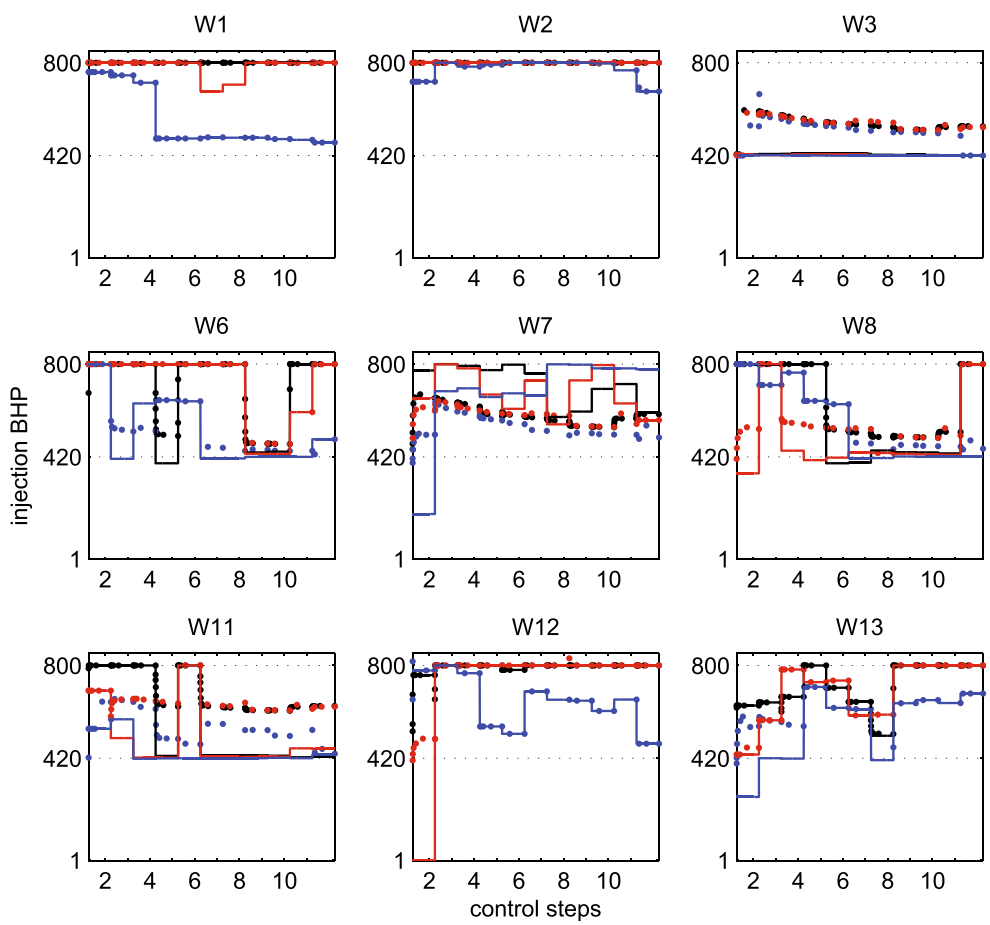

Fig. 10 Injection BHP optimal controls for optimization with constrained simulations; all simulations performed for small (*black*), medium (*red*), and large (*blue*) time step refinements after control update

6.2 Number of optimization iterations

One notices in Fig. 7 that the optimization with constrained simulations requires fewer gradient evaluations than the constrained optimization. It happens because, in SQP, linear model of nonlinear constraints (7) requires more frequent updates of the gradients to ensure feasibility. This is confirmed by the behavior of the optimal controls of the injection well W07, in Fig. 9. Here, the top plots contain both the target control values (solid lines) and actual values obtained in simulation (dots). The difference between the two curves indicates which control type has changed from BHP to phase flow rate, or where a well has been shut-in. The spacing of the dots corresponds to the actual time steps.

Figure 9a and c illustrate the effort of constrained optimization to satisfy the upper bound of the injection rate. We observe that when an extremely high rate occurs at the beginning of the control step, nonlinear constraints (7) become more sensitive to the changes in BHP control and the constraint gradient gets higher. It indicates that the time step approaches the transient time scale and it is, therefore, more difficult for a well control to satisfy those constraints. In Fig. 9c, it is exemplified by the rate corresponding to the small refinement scenario (black line) which has not converged to an optimal solution within an allocated number of gradient evaluations.

The optimization with constraint simulation results in a high injection due to the switching of injection control from BHP to phase flow rate, see Fig. 9d. The actual BHP values lie on a curve smoother than the target BHP values according to Fig. 9b.

6.3 Convergence failure in optimization

In this section, the focus is on the optimal solution corresponding to constrained simulations with the large refinement scenario. Two observations can be made about this solution. On the one hand, Fig. 7b indicates the early termination of the optimization algorithm. On the other hand, the optimization results lack consistency since their correlation with the small refinement solution is higher than the correlation with the medium one, see Fig. 8b. The combination of these observations indicates failure of the SQP algorithm. The origin of this failure can be traced once

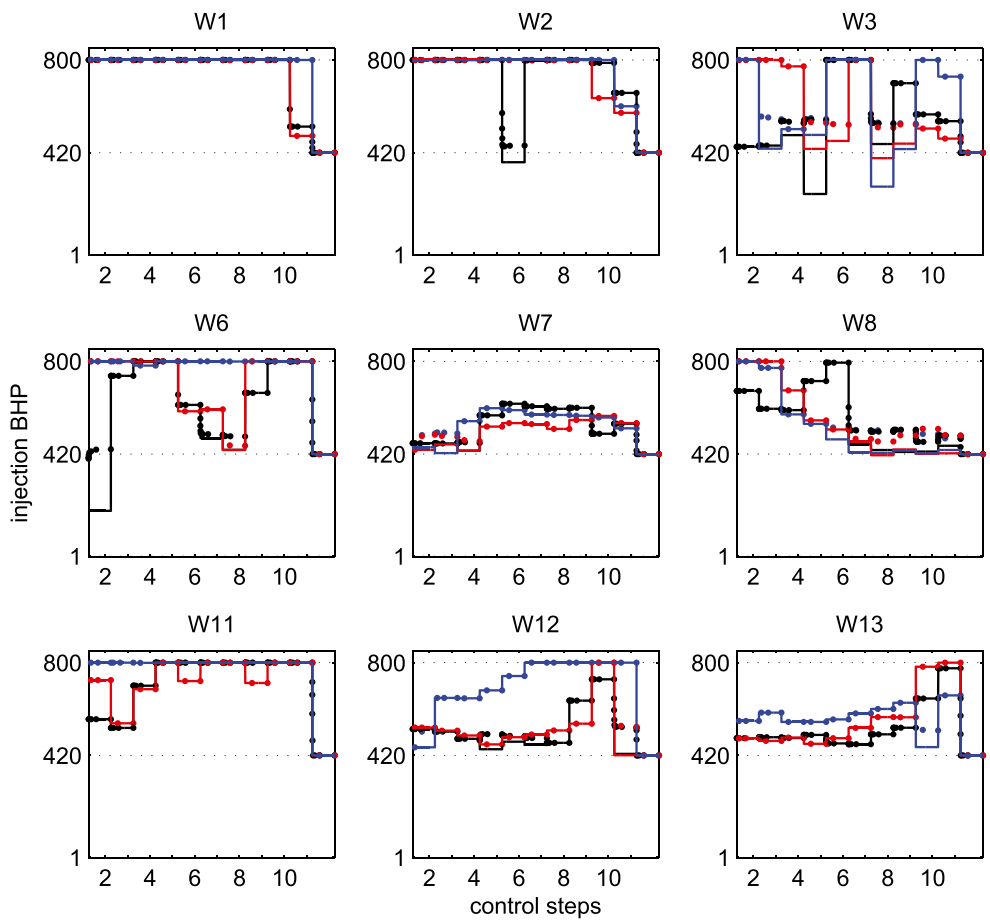

Fig. 11 Injection BHP optimal controls for constrained optimization; all simulations performed for small (*black*), medium (*red*), and large (*blue*) time step refinements after control update

the optimal BHP controls between the two constraining scenarios are compared. Figure 10 shows that the designed time step refinement is significantly violated for the case in question (blue line) with constrained simulations. According to the previous findings, it results in inconsistencies of the adjoint gradient sufficient to become an obstacle for the SQP algorithm. In comparison, the violation of the designed refinement is less prominent in constrained optimization, see Fig. 11.

7 Conclusions and recommendations

This paper focuses on how the time stepping strategy in reservoir simulation influences production optimization solutions performed with the adjoint gradient method and the SQP algorithm. Using a reservoir simulator featuring automatic differentiation and flexible time step refinement, it is shown that one must be cautious when using fully-implicit simulations with large time steps. In the BHP controlled production and injection, variations in the phase rate evaluation between different runs of the reservoir simulator affect the objective function value and adjoint gradients. As a result, the optimal solution becomes sensitive to time step refinement. These observations are supported by examples both in constrained and unconstrained production optimization.

In real field reservoir simulations, the well BHP controls are often paired with well flow rate constraints. The same strategy can also be applied to the SQP solver. In the second part of this paper, we studied how these two constraining strategies are affected by the time step refinement. In particular, we study the refinement occurred immediately after control update. Using an SPE10 test case, the robustness of both strategies is demonstrated when the maximum time step size after update varies from 32 days to 0.01 day. It is established that when nonlinear constraints are introduced in optimization, the NLP solver requires high number gradient evaluations to maintain the accuracy of the approximated constraints. As a result, the number of gradient computations doubled in comparison to optimization with constrained simulations. We emphasize that this observation is limited to the SQP algorithm that uses a linear approximation of nonlinear constraints. One may achieve faster convergence when using the NLP solver featuring a suitable nonlinear approximation of constraints.

In conclusion, when performing production optimization with the SQP solver, we recommend using the phase rate constraints in a simulation with a moderate time step refinement after control update.

Acknowledgments The authors would like to thank Professor Khalid Aziz for his contribution and advice on different aspects of this study. The authors also acknowledge funding provided by the industrial affiliates of SUPRI-B and Smart Fields Consortia.

Appendix A: Smooth approximation of the maximum function

In addition to Eq. 17a, two other approximations of the maximum function frequently used in continuous variable optimization [19] are

$$\max(a, b) \cong \frac{a\ \exp(a\,\kappa) + b\exp(b\,\kappa)}{\exp(a\,\kappa) + \exp(b\,\kappa)}, \tag{21a}$$

$$\max(a, b) \cong \frac{1}{\kappa}\ \log(\exp(a\,\kappa) + \exp(b\,\kappa)). \tag{21b}$$

Equations 21a and 21b require scaling parameter κ to be adjusted to the orders of magnitude of a and b. This requirement is twofold. On the one hand, the larger is the value of κ, the better is the approximation in 21a and 21b. On the other hand, because of the computational limits of the exponential function, overflow and underflow errors may occur if the argument is above the limit dictated by the machine precision. Unlike Eqs. 21a and 21b, Eq. 17a needs parameter adjustment only for small values of the arguments a and b. Therefore, Eq. 17a seems more suitable for the production optimization.

In addition, when the arguments a and b differ by a small amount, Eq. 17a yields more accurate approximation of the values and derivatives of the function than Eqs. 21a and 21b. For example, an input of $a = 100$, $b = 101$ results in 101.000002, 100.999071, and 101.000133 for Eqs. 17a, 21a and 21b, respectively. Here, we select $\kappa = 6.981$ to be the most suited value in double precision, whereas $\varepsilon = 10^{-5}$. Partial derivatives of the functions in Eqs. 17a, 21a, 21b are respectively 2.49998×10^{-6}, $-0.0055474 \times 10^{-3}$, $0.00092851 \times 10^{-4}$ for a and 0.999998, 1.00555, and 0.999071 for b.

References

1. Brouwer, D., Jansen, J.D.: Dynamic optimization of waterflooding with smart wells using optimal control theory. SPE J. **9**(4), 391–402 (2004)
2. Bukshtynov, V., Volkov, O., Durlofsky, L., Aziz, K.: Comprehensive framework for gradient-based optimization in closed-loop reservoir management. Comput. Geosci. **19**(4), 877–897 (2015)
3. Cao, H.: Development of techniques for general purpose simulators. PhD Thesis, Stanford University (2002)
4. Carter, R.: Numerical experience with a class of algorithms for nonlinear optimization using inexact function and gradient information. SIAM J. Sci. Comput. **14**, 368–388 (1993)

5. Christie, M., Blunt, M.: Tenth SPE comparative solution project: a comparison of upscaling techniques, SPE72469-PA. SPE Reserv. Eval. Eng. **4**(4), 308–316 (2001)
6. Coats, K.: An equation of state compositional model. SPE J. **20**(5), 363–376 (1980)
7. Geoquest: Eclipse Technical Description 2005A. Schlumberger (2005)
8. Gill, P.E., Murray, W., Saunders, M.: SNOPT: an SQP algorithm for large-scale constrained optimization. SIAM J. Optim. **12**(4), 979–1006 (2002)
9. Griesse, R., Walther, A.: Evaluating gradients in optimal control: Continuous adjoints versus automatic differentiation. J. Optim. Theory Appl. **122**(2), 63–86 (2004)
10. Gunzburger, M.: Perspectives in flow control and optimization. SIAM, Philadelphia (2003)
11. Iranshahr, A., Voskov, D., Tchelepi, H.A.: Tie-simplex parameterization for eos-based thermal compositional simulation. SPE J. **15**(2), 537–548 (2010)
12. Jiang, Y.: Techniques for modeling complex reservoirs and advanced wells. PhD Thesis, Stanford University (2007)
13. Karush, W.: Minima of functions of several variables with inequalities as side conditions. In: M.Sc. Dissertation, University of Chicago, Chicago, Chicago, IL, USA (1939)
14. Kourounis, D., Durlofsky, L., Jansen, J., Aziz, K.: Adjoint formulation and constraint handling for gradient-based optimization of compositional reservoir flow. Comput. Geosci. **18**(2), 117–137 (2014)
15. Kourounis, D., Voskov, D., Aziz, K.: Discrete and continuous adjoint formulations for optimization of compositional flow. In: Proceedings of ECMOR XII European Conference on the Mathematics of Oil Recovery (2010)
16. Kraaijevanger, J., Egberts, P., Valstar, J., Buurman, H.: Optimal waterflood design using the adjoint method, SPE105764-MS. In: Proceedings of SPE Reservoir Simulation Symposium (2007)
17. Muskat, M., Wyckoff, R.: The flow of homogeneous fluids through porous media. J.W. Edwards Inc., Ann Arbor, Michigan (1946)
18. Nocedal, J., Wright, S.J. Numerical optimization, 2nd edn. Springer, New York (2006)
19. Polyak, R.: Smooth optimization methods for minimax problems. SIAM J. Control. Optim. **26**(6), 1274–1286 (1988)
20. Sarma, P., Durlofsky, L.J., Aziz, K., Chen, W.H.: Efficient real-time reservoir management using adjoint-based optimal control and model updating. Comput. Geosci. **10**(1), 3–36 (2006)
21. Süli, E., Mayers, D.: An introduction to numerical analysis. Cambridge University Press, New York (2003)
22. Tchelepi, H., Zhou, Y.: Multi-GPU parallelization of nested factorization for solving large linear systems, SPE163588-MS. In: Proceedings of SPE Reservoir Simulation Symposium (2013)
23. Van Essen, G., Zandvliet, M., Van Den Hof, P., Bosgra, O., Jansen, J.: Robust waterflooding optimization of multiple geological scenarios. SPE J. **14**(1), 202–210 (2009)
24. Volkov, O., Kourounis, D.: Optimization module of AD-GPRS. Technical documentation, Department of Petroleum Engineering, Stanford University (2013)
25. Volkov, O., Voskov, D.: Advanced strategies of forward simulation for adjoint-based optimization, SPE163592-MS. In: Proceedings of SPE Reservoir Simulation Symposium (2013)
26. Voskov, D., Zhou, Y.: Technical description of AD-GPRS (2012). https://pangea.stanford.edu/researchgroups/supri-b/research/research-areas/gprs
27. Voskov, D.V., Tchelepi, H.A.: Compositional nonlinear solver based on trust regions of the flux function along key tie-lines, SPE141743-MS. In: Proceedings of SPE Reservoir Simulation Symposium (2011)
28. Voskov, D.V., Tchelepi, H.A.: Comparison of nonlinear formulations for two-phase multi-component EoS based simulation. J. Pet. Sci. Eng. **82-83**, 101–111 (2012)
29. Wallis, J.: Incomplete gaussian elimination as a preconditioning for generalized conjugate gradient acceleration, SPE12265-MS. In: Proceedings of SPE Reservoir Simulation Symposium (1983)
30. Wang, X.: Trust-Region Newton Solver for Multiphase Flow and Transport in Porous Media. PhD Thesis, Stanford University (2012)
31. Younis, R.: Modern advances in software and solution algorithms for reservoir simulation. PhD Thesis, Stanford University (2011)
32. Younis, R., Tchelepi, H., Aziz, K.: Adaptively localized continuation-newton method–nonlinear solvers that converge all the time. SPE J. **15**(2), 526–544 (2010)
33. Zaydullin, R., Voskov, D., James, S., Lucia, A.: Fully compositional and thermal reservoir simulation. Comput. Chem. Eng. **63**, 51–65 (2014)
34. Zaydullin, R., Voskov, D.V., Tchelepi, H.A.: Nonlinear formulation based on an equation-of-state free method for compositional flow simulation. SPE J. **18**(2), 264–273 (2012)
35. Zhou, Y.: Parallel general-purpose reservoir simulation with coupled reservoir models and multi-segment wells. PhD Thesis, Stanford University (2012)
36. Zhou, Y., Tchelepi, H., Mallison, B.: Automatic differentiation framework for compositional simulation on unstructured grids with multi-point discretization schemes, SPE141592-MS. In: Proceedings of SPE Reservoir Simulation Symposium (2011)